Control of the oxygen to ocean heat content ratio during deep convection events

Daoxun Sun[1], Takamitsu Ito[1], Annalisa Bracco[1]and Curtis Deutsch[2]

[1]School of Earth and Atmospheric Sciences, Georgia Institute of Technology, Atlanta, Georgia, U.S.A.

[2]School of Oceanography, University of Washington, Seattle, Washington, U.S.A

Key Points:

- A hierarchy of models are used to examine the factors controlling the ratio between oxygen uptake and the heat loss (O_2-OHC ratio) at high latitudes.
- The O_2-OHC ratio of individual convective events depend on both the surface forcing and the pre-conditioning of subsurface properties.
- The vertical gradients of dissolved oxygen and temperature are essential for the the O_2-OHC ratio associated with the interannual variability.

Corresponding author: Daoxun Sun, `daoxun.sun@eas.gatech.edu`

Abstract

Earth System Models project a decline of dissolved oxygen in the oceans under warming climate. Observational studies suggest that the ratio of O_2 inventory to ocean heat content (O_2-OHC) is several fold larger than can be explained by solubility alone, but the ratio remains poorly understood. In this work, models of different complexity are used to understand the factors controlling the O_2-OHC ratio during deep convection, with a focus on the Labrador Sea, a site of deep water formation in the North Atlantic Ocean. A simple one-dimensional convective adjustment model suggests two limit case scenarios. When the near-surface oxygen level is dominated by the entrainment of subsurface water, surface buoyancy forcing , air-sea gas exchange coefficient and vertical structure of sea water together affect the O_2-OHC ratio. In contrast, vertical gradients of temperature and oxygen become important when the surface oxygen flux dominates. The former describes the O_2-OHC ratio of individual convective event in agreement with model simulations of deep convection. The latter captures the O_2-OHC ratio of interannual variability, where the pre-conditioning of interior ocean gradients dominates. The relative vertical gradients of temperature and oxygen, which in turn depend on the lateral transport and regional biological productivity, control the year-to-year variations of O_2-OHC ratio. These theoretical predictions are tested against the output of a three-dimensional regional circulation and biogeochemistry model which captures the observed large-scale distribution of the O_2-OHC ratio, and agrees broadly with the prediction by the simpler model.

Plain Language Summary

Numerical simulations suggest that the dissolved oxygen (O_2) in the ocean will continue decreasing in the ocean under warming climate. An important metric for this problem is the ratio between the oxygen loss and climate warming, in particular, for the high latitude oceans. Vast majority of the waters in the oceans are stored in the mid-depth and deep oceans, thus heat and oxygen as well. As the O_2 in deep ocean can only be supplied from the surface during deep mixing events at high latitudes in the cold season, it is important to know how much oxygen can enter the ocean for a given amount of cooling in order to understand the relationship between oxygen loss and global warming in the ocean interior. This study investigates the ratio between oxygen uptake and heat loss (O_2-OHC ratio) during deep winter mixing events using models of different complexi-

ties. Our results suggest that this ratio differs under different cooling scenarios. The physical property changes of the water column at the convection site are essential to determine the O_2-OHC ratio. The larger the difference in O_2 concentration between the surface and the deep ocean, the greater the amplitude of the O2-OHC ratio, which we call "preconditioning". Under global warming, the stratification of the ocean surface will increase and this will reduce the magnitude of the ratio.

1 Introduction

Dissolved oxygen (O_2) is essential for living organisms in the marine ecosystem. (e.g., Codispoti, 1995; Morel & Price, 2003; Pörtner & Knust, 2007). However, both projections by Earth System Models (ESMs) and observational data suggest that O_2 in the global oceans has declined in recent decades and will continue to do so under a warming climate (Bopp et al., 2002; Matear et al., 2000; Plattner et al., 2002; Keeling et al., 2010; Schmidtko et al., 2017). Warming has two main effects on the oceanic oxygen inventory. First, the increasing temperature directly reduces oxygen solubility. Secondly, warming of the upper ocean increases the stratification and indirectly impact oxygen availability. This increase on one hand weakens the exchange between the well-oxygenated surface water and the ocean interior, and on the other hand reduces the upwelling of nutrients from the deep ocean, slowing the respiratory consumption of O_2 through reduced organic matter export to the subsurface. Globally, stronger stratification decreases O_2, and the net result is that warming and increasing stratification work together to deplete oxygen in the ocean (Bopp et al., 2002; Plattner et al., 2002).

The loss of oxygen per unit heat uptake, defined as the oxygen to ocean heat content (O_2-OHC) ratio, is a metric that has been used to quantify ocean deoxygenation. Keeling and Garcia (2002) suggested that the natural O_2-OHC ratio spans a wide range from -2 to -10 $nmolO_2\,J^{-1}$ based on the mean seasonal cycle of air-sea O_2 fluxes. Larger ratios are typically found at higher latitudes and when averaged over longer time scales. ESMs have predicted that the O_2-OHC ratio at the end of this century in global warming scenarios will be between -5.9 and -6.7 $nmolO_2\,J^{-1}$ (Keeling et al., 2010). Ito et al. (2017) estimated the O_2-OHC ratio of the upper ocean (0-1000 m) as -8.2 $\pm$ 0.7 $nmolO_2\,J^{-1}$ based on historic data from 1958 to 2015 (Fig. 1). For the surface layers, the O_2-OHC ratio follows the dependency of solubility on temperature change, but when deeper layers are included, the ratio is much larger than what can be explained by the solubility
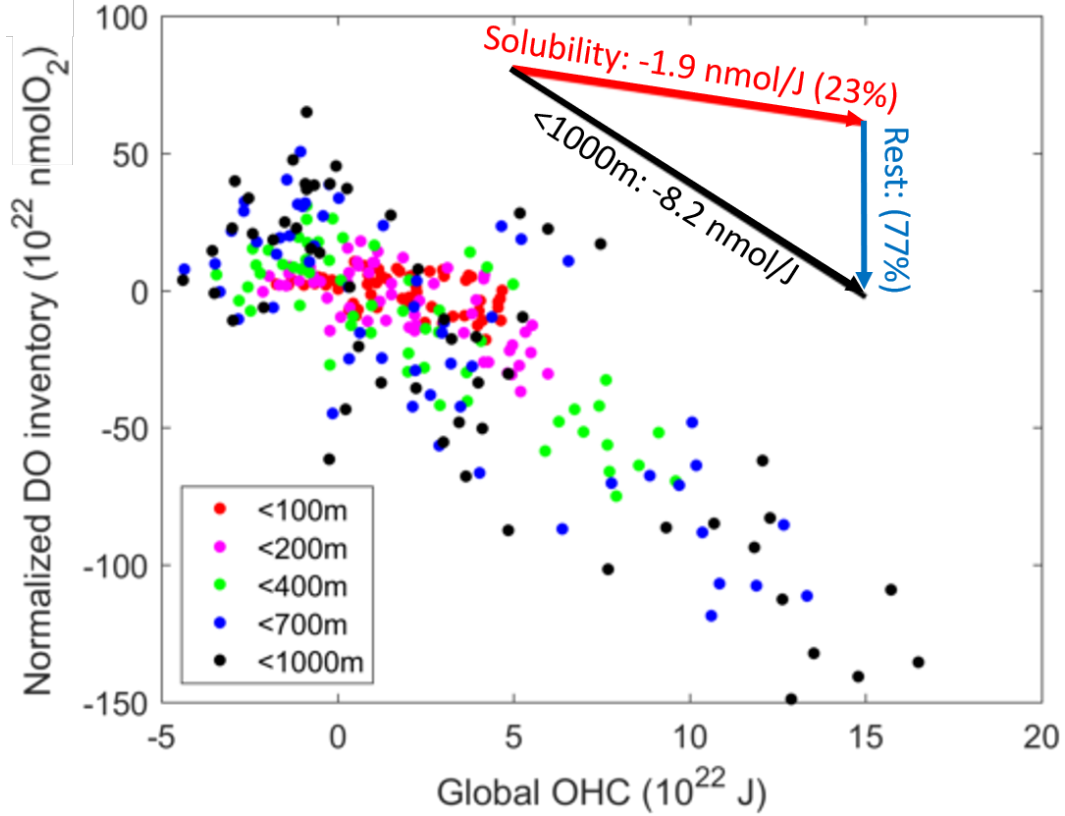
Figure 1. Normalized oxygen inventory as a function of global OHC inventory from 1858 to 2013 with the 1960-1970 decadal average removed from Ito et al. (2017). Dots with different colors indicate annual anomalies of oxygen inventories and OHCs from different depth ranges. The black arrow shows the slope between oxygen inventory and OHC for the upper 1,000 m in the global ocean. The red arrow shows the slope based on the solubility, and the blue arrow shows the residual.

change alone. The percentage of the ratio explained by solubility for the upper 1000 m of the global ocean is indeed only 23%. The remaining portion must result from the ocean circulation and biological cycling (Keeling & Garcia, 2002). In this work, we investigate the O_2-OHC ratio by examining the relationship between heat loss and oxygen uptake at a site of deep water formation, and the factors that constrain this ratio.

The oxygen is physically supplied in large amounts to the ocean interior from the high latitudes where the water subducts during the cold season (Körtzinger et al., 2004). Near-surface physical processes determine the O_2 content at the time of deep water formation, known as preformed oxygen (Ito et al., 2004). While cooling raises oxygen sol-

ubility, convective mixing and entrainment lower the preformed oxygen, overall generating a strong oxygen flux into the ocean. The heat loss and oxygen uptake during this process set the ratio between the preformed oxygen and OHC. In this study, the Labrador Sea, a well sampled deep water formation site (Clarke & Gascard, 1983; Gascard & Clarke, 1983; Marshall & Schott, 1999; Lazier et al., 2002; Pickart et al., 2002; Yashayaev et al., 2007; Yashayaev, 2007), is chosen as a representative location to examine the relationship between oxygen flux and surface buoyancy forcing. Winter convection in this basin generates the well oxygenated Labrador Sea Water (LSW) that then spreads across the northwest Atlantic between 1,000 and 2,200 m (Talley & McCartney, 1982; Hall et al., 2007). Therefore, the O_2-OHC ratio of the newly formed LSW can influence the entire North Atlantic, and the underlying processes may be relevant to other regions where deep convection occurs.

In this work, we investigate the sensitivity of oxygen uptake to heat loss using a hierarchy of models. In section 2 we develop hypotheses using a one-dimensional (1-D) convective adjustment model forced by surface cooling. Based on this idealized model, we derive theoretical predictions for the O_2-OHC ratio. In section 3 we design a set of numerical simulations to test our theory. The results of the simulations are analyzed in Section 4. Section 5 summarizes the main findings.

2 Theory and hypotheses

Fig. 2 schematically illustrates the processes at play. Heat loss at the ocean surface (Q) is the principal driver of ocean oxygen uptake (Sun et al., 2017). Firstly, atmospheric cooling decreases the upper ocean temperature and increases the solubility. This causes surface undersaturation and the diffusive gas transfer increases oxygen at the surface. Secondly, cooling causes convective instability. The intense vertical mixing brings up deep waters that are undersaturated in oxygen due to the cumulative effect of respiration. This further enhances the oxygen undersaturation and uptake at the surface. The oxygen uptake reduces the magnitude of undersaturation as the air-sea exchange brings the surface water towards saturation.

Sun et al. (2017) showed that, for a given amount of heat loss, the net oxygen uptake depends on the duration and intensity of the cooling event, and details of cooling conditions can lead to different O_2-OHC ratios. To illustrate this dynamics, we construct
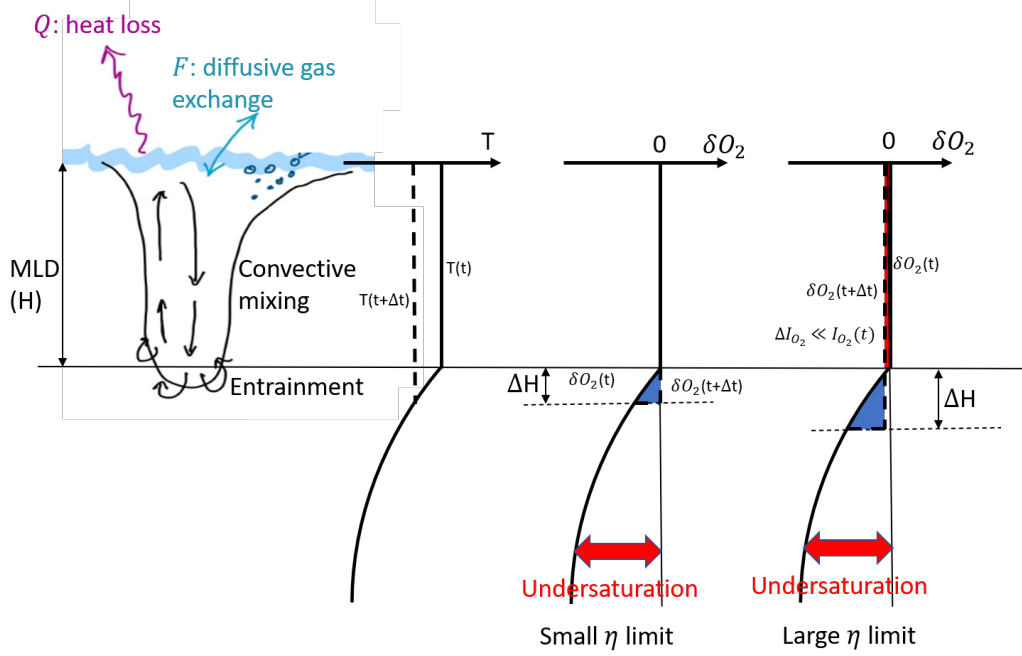
Figure 2. Schematic diagram of physical processes that control oxygen fluxes during winter time convection. $\delta O_2 = [O_2] - [O_{2,sat}]$ is a measure of saturation, and is generally negative in the interior ocean due to the cumulative effect of respiration. The three profiles illustrates the changes in temperature (left) and oxygen saturation (center and right) under two limit case scenarios. Solid lines indicate the initial state, and dash lines show the state after the mixed layer deepening of ΔH. Blue shadings in the δO_2 profiles represent the increase in δO_2, while the red shadings indicate decreases. When the surface oxygen flux is strong and the oxygen tendency due to the entrainment is negligible (small η limit, center), the mixed layer δO_2 remains zero due to the relatively strong gas exchange. When the entrainment is dominant and surface oxygen flux is negligible (large η limit, right), the mixing only re-distribute δO_2, leading to no net change in column O_2 inventory.

117   a simple vertical 1-D model to examine the factors that control oxygen uptake and vari-

118   ability of air-sea O_2 disequilibrium during convective mixing. This model also allows to

119   develop theoretical predictions about the relationship between the rate of surface cool-

120   ing and oxygen gain, thus the O_2-OHC ratio.

121   In this idealized model, we neglect horizontal transport and assume that vertical

122   mixing is induced by convection. All properties are assumed to be well mixed within the

123   mixed layer, but all properties remain the same as the initial conditions below the mixed

124   layer. Mixed layer depth (MLD) only increases when the stratification is unstable at the

125   bottom of the mixed layer (i.e., the water in the mixed layer is less buoyant than the wa-

126   ter beneath).

127   In this framework, there are two definitions of the O_2-OHC ratio. The first is the

128   O_2-OHC ratio of a single convective event or the seasonal O_2-OHC ratio, which can be

129   calculated by dividing the total oxygen uptake by the total heat loss, integrating over

130   a convective event. Graphically, it is the y/x ratio if O_2 content is plotted as y against

131   OHC as x. The second definition applies to the interannual change in O_2-OHC ratio among

132   different winters. For example, the mean December-January-February (DJF) heat and

133   O_2 fluxes can vary interannually, with some years having stronger cooling and more O_2

134   gain. Interannual O_2-OHC ratio can be calculated as the regression coefficient of the to-

135   tal oxygen uptake as a function of OHC. Thus, it is the sensitivity of oxygen content to

136   the changes in OHC regardless of the background, mean-state O_2-OHC ratio. Graph-

137   ically, the interannual ratio would be dy/dx, if again O_2 content is plotted against OHC.

138   ## 2.1 1-D convective model

139   For simplicity, we assume that the ocean stratification is controlled entirely by the

140   temperature gradient, and only consider the diffusive gas exchange at the surface for the

141   air-sea oxygen exchange. The detailed derivation can be found in the Supporting Infor-

142   mation, and here we only describe the main characteristics of the 1-D model solutions.

143   First let us consider the heat balance of the mixed layer under cooling condition

144   as illustrated in Fig 2 (left). Under the above assumptions, the mixed layer depth (MLD),

145    $H(t)$, is related to the initial potential temperature profile, $T_0(z)$, and to the heat flux,

146    $Q(t)$, at the surface according to:

$$\frac{dH^2}{dt} = -\frac{2Q(t)}{\rho_0 C_p}\left(\frac{dT_0}{dz}\right)^{-1},\tag{1}$$

147   where ρ_0 and C_p are the reference density and specific heat of sea water. The evolution

148   of the square of MLD is proportional to the rate of heat loss and inversely proportional

149   to the initial stratification. This relationship is only applicable under cooling conditions

150   ($Q < 0$) and increasing H. When the water column is heated, the stratification imme-

151   diately develops at the surface and this simple model cannot represent the sudden shoal-

152   ing of the MLD.

153   To directly relate the oxygen level and the air-sea gas flux, we introduce $\delta O_2(t) =$

154    $O_2(t) - O_{2,sat}(T(t))$ as a prognostic variable reflecting the oxygen saturation state. We

155   assume constant salinity and a temperature-only dependency for solubility. Then the dif-

156   fusive oxygen flux can be written as

$$F = -G\delta O_2,\tag{2}$$

157   where G is diffusive gas exchange coefficient. The δO_2 budget in the mixed layer is:

$$H\frac{d\delta O_2}{dt} = -\left\{\delta O_2 - \delta O_{2,0}(-H)\right\}\frac{dH}{dt} + F - \frac{AQ}{\rho_0 C_p},\tag{3}$$

158   where $\delta O_{2,0}(z)$ is the initial δO_2 profile, F is the surface air-sea oxygen flux, and $A =$

159    $\partial O_{2,sat}/\partial T$. The left hand side (LHS) is the oxygen saturation change in the mixed layer.

160   The first term on the right hand side (RHS) describes the entrainment of subsurface δO_2,

161   the second is the air-sea exchange, and the third is the solubility change due to the air-

162   sea heat flux. Given the initial profile of T and O_2, we can calculate the initial profile

163   of δO_2. This equation can be numerically integrated using Eq.1 forced by the air-sea heat

164   flux, Q. Additionally, under certain limit-case scenarios, we can obtain the analytical so-

165   lutions that provide some insight into the system behavior. In this convective model, the

166   surface oxygen flux and the entrainmentment at the bottom of mixed layer determine

167   the oxygen concentration in the mixed layer. Here we use a dimension-less number $\eta =$

168    $G^{-1}\left(\frac{dH}{dt}\right)$ to quantify the relative strength of the entrainment and surface oxygen flux.

169   We will look into the behavior of the system when η is small (surface flux dominates)

170   or large (entrainment dominates).

171 **2.2 Case 1: small η limit**

172 First, we explore the limit-case scenario where Eq. 3 is dominated by the diffusive

173 gas exchange. This scenario is depicted in the center profile in Fig 2. In this case, the

174 deepening of mixed layer is relatively slow compared to the air-sea equilibration of O_2,

175 so surface oxygen remains close to saturation, $\delta O_2 \sim 0$. Graphically, this case assumes

176 that the O_2 deficit entrained from the subsurface is replenished by the air-sea gas trans-

177 fer. Thus, the total integrated heat flux (I_Q) and oxygen flux (I_{O_2}) can be determined

178 by the heat and δO_2 budget for the water column:

$$I_Q = \int_0^t Q(t')dt' = \rho_0 C_p \left\{ T_0(-H)H(t) - \int_{-H(t)}^0 T_0(z)dz \right\}. \tag{4}$$

179

$$I_{O_2} = \int_0^t F(t')dt' = -\int_{-H(t)}^0 \delta O_{2,0}(z)dz + A\frac{I_Q}{\rho_0 C_p}. \tag{5}$$

180 If we further simplify the problem by assuming that these profiles are linear, then the

181 seasonal and interannual O_2-OHC ratios can be identically obtained as

$$\frac{I_{O_2}}{I_Q} = \frac{dI_{O_2}}{dI_Q} = -\frac{1}{\rho_0 C_p}\left(\frac{k_{\delta O2}}{k_T} - A\right), \tag{6}$$

182 where $k_{\delta O2}$ and k_T are the vertical gradient of $\delta O_{2,0}(z)$ (assuming $\delta O_{2,0}(0) = 0$) and

183 $T_0(z)$. Usually potential temperature and δO_2 both decrease from the surface downwards,

184 which means $\frac{k_{\delta O2}}{k_T} > 0$, and $A < 0$, so $\frac{I_{O_2}}{I_Q} < 0$. In this limit case scenario, the O_2-

185 OHC ratio is independent of the strength of the surface heat flux as long as the convec-

186 tive mixing is relatively weak and surface waters remain well equilibrated. The O_2-OHC

187 ratio depends on the relative strength between the vertical gradients of δO_2 and poten-

188 tial temperature, $\frac{k_{\delta O2}}{k_T}$. A larger value of $\frac{k_{\delta O2}}{k_T}$ implies a stronger entrainment of δO_2, lead-

189 ing to more oxygen uptake from the atmosphere, for the same amount of heat loss.

190 The vertical gradient of δO_2 is a preconditioning factor, regulating how much un-

191 dersaturation can potentially occur if the stratified water column is distablized. The small

192 η limit is a limit-case scenario because the relatively slow entrainment ensures that dif-

193 fusive gas exchange can fully supply O_2 to bring the entire mixed layer to equilibrium.

194 The total oxygen uptake is eventually determined by the saturation state of the subsur-

195 face water before the convection starts (pre-conditioning) and by the depth the mixed

196 layer at the end of the convective event. The entrainment flux of negative δO_2 is fully

197 compensated by the air-sea gas flux, resulting in the largest possible O_2-OHC ratio. Note

198 that subsurface undersaturation is identical to the apparent oxygen utilization (AOU),

199 such that the preconditioning of δO_2 below the mixed layer reflects the biological O_2 con-

200 sumption. Strong biological activity leads to a strong vertical gradient of δO_2 and a po-

201 tentially larger O_2-OHC ratio. The real O_2-OHC ratio will be smaller than this extreme

202 case since the surface water is likely undersaturated during convective events.

2.3 Case 2: large η limit

203

204 In the other limit-case scenario, δO_2 is dominated by the entrainment of subsur-

205 face water, and the air-sea gas exchange does not affect the mixed layer δO_2. In this limit,

206 the integral δO_2 balance is set by the entrainment of subsurface waters and the cooling-

207 induced solubility increase. Once the δO_2 is calculated, then the air-sea gas exchange

208 can be diagnosed as:

$$F(t) = -\frac{G}{H(t)} \left\{ \int_{-H(t)}^{0} \delta O_{2,0}(z)dz - \frac{A}{\rho_0 C_p} I_Q \right\}. \tag{7}$$

209 The first term on the RHS represents the effect of vertical mixing on the δO_2, averag-

210 ing over the mixed layer. This drives the diffusive air-sea O_2 flux into the ocean. The

211 second term on the RHS reflects the additional diffusive O_2 uptake due to the solubil-

212 ity increase under the cooling.

213 Again, a simple solution can be obtained by assuming linear initial profiles and a

214 constant heat flux ($I_Q = Qt$). Then H(t) can be calcualted from Eq. 1 and 7, yield-

215 ing a theoretical prediction for I_{O_2}:

$$I_{O_2} = \frac{G}{3}(\frac{2k_T}{\rho_0 C_p})^{1/2}(\frac{k_{\delta O2}}{k_T} - A)(-Q)^{1/2}t^{3/2}. \tag{8}$$

216 Then the seasonal O_2-OHC ratio becomes

$$\frac{I_{O_2}}{I_Q} = -\frac{G}{3} \left(\frac{2k_T\,t}{-\rho_0\,C_p\,Q} \right)^{1/2} \left(\frac{k_{\delta O_2}}{k_T} - A \right). \tag{9}$$

217 Similar to the small η assumption, $\frac{I_{O_2}}{I_Q}$ is always negative given that $\frac{k_{\delta O2}}{k_T} > 0$. The fac-

218 tor $(\frac{t}{-Q})^{1/2}$ on the RHS of Eq. 9 indicates that the O_2-OHC ratio depends on how the

219 cooling is applied.

220 In this limit case scenario, the intense mixing prevents the full air-sea equilibra-

221 tion of O_2 in the mixed layer, and the resulting O_2-OHC ratio is modulated by the mag-

222 nitude δO_2 as well as the duration of cooling event which controls for how long the air-

223 sea gas transfer can occur. For a given length of the cooling period, the O_2-OHC ratio

224 is larger when the cooling is less intense. For a fixed amount of heat loss, the O_2-OHC

ratio is larger when the cooling is applied over a longer period. The O_2-OHC ratio depends again on the initial gradient of δO_2 and potential temperature, but the relation is more complicated compared to the small η limit. The diffusive gas exchange is determined by the δO_2 value in the mixed layer driven by the entrainment from the subsurface layer. $\frac{k_{\delta O2}}{k_T}$ controls how much the δO_2 of the whole mixed layer will decrease for a given heat loss, but the MLD can also affect the averaged δO_2 in the mixed layer. For the same amount of entrainment, δO_2 will decrease more in a shallow mixed layer than in a deep one.

Determining the interannual O_2-OHC ratio is complicated here since both the cooling rate and the duration of the convective events can vary between different years. If we compare the same winter month over different years, we can assume that the cooling duration is constant. Then the interannual O_2-OHC ratio is given by

$$\frac{dI_{O_2}}{dI_Q} = -\frac{G}{3}\left(\frac{k_T}{2\rho_0 C_p}\right)^{1/2}\left(\frac{k_{\delta O2}}{k_T} - A\right)\frac{t}{(-Qt)^{1/2}}. \tag{10}$$

Being proportional to $(-Q)^{-1/2}$, the ratio is smaller for stronger cooling. This situation again represents an upper limit to the real O_2-OHC ratio since the diffusive gas exchange will be reduced once the surface O_2 concentration increases due to the surface uptake, which is not included here.

2.4 Hypotheses

Building on these theoretical developments we hypothesize that three independent factors control the O_2-OHC ratio, and their relative importance may depend on the timescale considered:

- The temperature sensitivity of O_2 solubility, $A = \partial O_{2,sat}/\partial T$.
- The stratification of temperature and oxygen saturation, $k_{\delta O_2}/k_T$.
- The surface buoyancy forcing, Q and t, and gas exchange rate, G.

The small η limit of Eq. 6 contains the full expression of these two mechanisms ($k_{\delta O_2}/k_T - A$). Note that A is a negative number, so these two terms reinforce each other. The large η limit of Eq. 9 and 10 reflects the same processes, but under the limitation of a finite gas exchange.

Numerical solutions of the 1-D convective adjustment model under different surface cooling rates are shown in Fig. 3. Here the model is integrated from a linear profile of $T_0(z)$ and $\delta O_{2,0}(z)$ with $k_T = 1 \times 10^{-3} \,^oC\,m^{-1}$ and $k_{\delta O2} = 4 \times 10^{-2} mmol\,m^{-4}$. These values broadly represent the vertical gradients in the Labrador Sea. We also use a constant gas transfer velocity $G = 1.45 \times 10^{-4} m\,s^{-1}$. With these parameter choices, both limit case solutions are similar to the numerical solution to Eqs. 1 and 3 when the cooling rate is weak ($\sim$ -50 W/m^2). As expected, under a stronger cooling, numerical solutions are closer to the large η case (green line in Fig. 3). The stronger cooling drives more intense deeper mixing such that air-sea gas exchange cannot maintain the surface water in equilibrium with the atmosphere. The solubility contribution, $A/(\rho_0\,C_p)$, represents the change in oxygen solubility due to cooling, and is indicated by the black line in Fig. 3. The simulated O$_2$ flux is always stronger than this solubility effect.

The seasonal O$_2$-OHC ratio would be equivalent to picking a point in Fig. 3 and evaluating $\frac{\bar{F}}{\bar{Q}}$, while the interannual change in the O$_2$-OHC ratio can be calculated as the local slope, $\frac{d\bar{F}}{d\bar{Q}}$. The solution shows the negative relationship between loss of heat and gain of oxygen, as stronger heat loss leads to an increase in oxygen uptake. The small η limit exhibits a strong linear relationship between heat and oxygen fluxes. When the cooling is strong during convective events, the behavior of the oxygen uptake is better approximated by the large η limit because near surface O$_2$ is under-saturated due to the mixing of deep water to the surface, and the air-sea gas exchange is not fast enough to bring the mixed layer to saturation.

3 Model hierarchy and experimental design

The theoretical developments presented so far predicted a range of O$_2$-OHC ratio in the context of a vertical 1-D water column model under intense cooling and convective mixing. In addition to the temperature-solubility relationship, the theory accounts for the effects of vertical gradients of O$_2$ and temperature, and incomplete air-sea gas exchange. In order to evaluate the theoretical prediction, we directly simulate ocean convection and air-sea gas transfer using a hierarchy of models. We compare the solutions of the 1-D convective adjustment model integrated numerically under different conditions with outputs from:

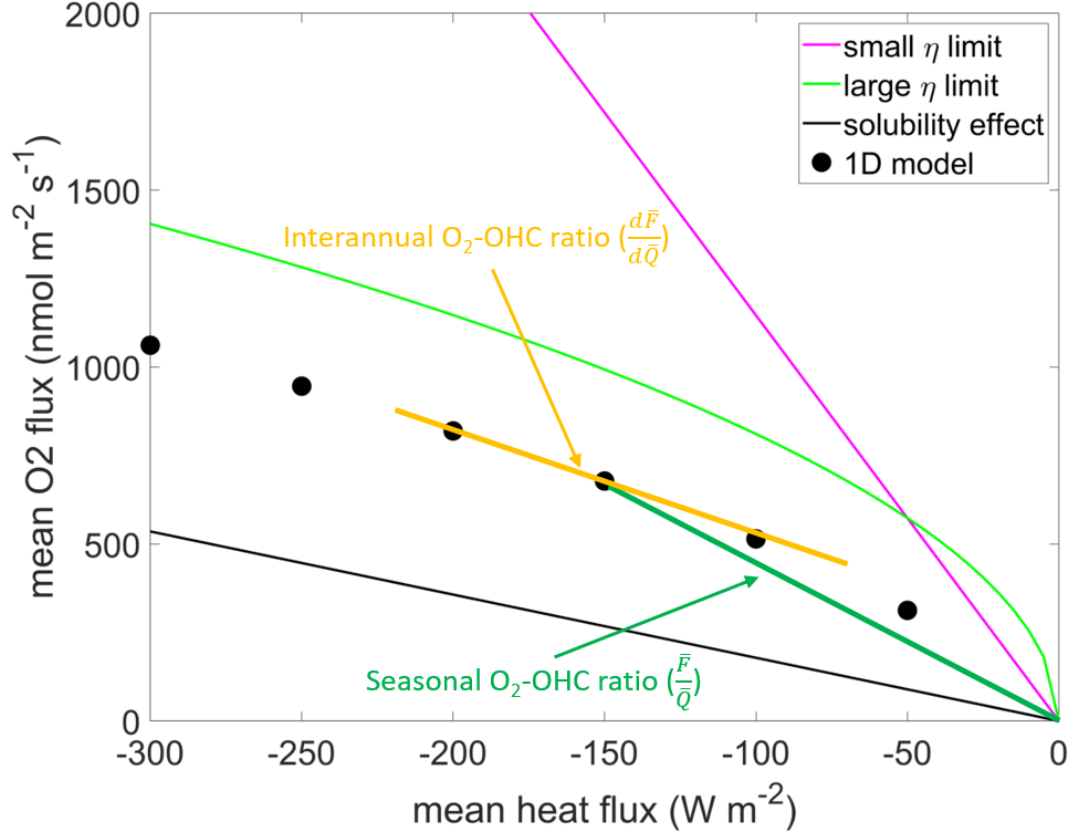- a non-hydrostatic simulation of deep convection episodes

Figure 3. Numerical solution of the 1-D convective adjustment model under different cooling rates and for different extreme cases. See text for the parameters of the 1-D convective adjustment model. The dark green line from the origin represents a convective event, with a slope of seasonal O_2-OHC ratio. The yellow line indicates the linear regression line around the selected convective event, slope of which represents the interannual O_2-OHC ratio.

- a regional, hydrostatic three-dimensional (3-D) simulation of Labrador Sea convection

The vertical 1-D model in the previous section represents the simplest possible set-up. At the next level, we use a non-hydrostatic model to directly simulate the deep convection in an idealized doubly periodic domain and calculate the vertical exchange of oxygen in the convective plumes at the horizontal resolution of 250 m. This model is abiotic, as the 1-D model, and is only integrated over a winter season. Finally, we use a regional 3-D model of ocean circulation and biogeochemistry configured for the Labrador Sea at the nominal horizontal resolution of 7.5 km. This model includes realistic ocean bathymetry, ecosystem and biogeochemical parameterizations, and open lateral boundary conditions nudged to reanalysis data. It is computationally expensive, but is realistic, and its output can be directly compared to the available observations. In all three types of simulations, the effect of bubble mediated gas flux is also tested, but for simplicity, we will mainly focus our discussion on the runs without bubble flux. The results from the runs with bubble injection activated are shown in the Supporting Information, and a brief discussion on the impact of the bubble flux is included in the discussion section.

3.1 Non-hydrostatic simulations

We first evaluate the theoretical prediction against a set of sensitivity simulations presented in Sun et al. (2017). These experiments are performed using the Massachusetts Institute of Technology General Circulation Model (MITgcm) (Marshall, Hill, et al., 1997; Marshall, Adcroft, et al., 1997) configured to allow non-hydrostatic dynamics and to explicitly resolve ocean deep convection (Jones & Marshall, 1993).

The model domain is a 32 km $\times$ 32 km box with periodic boundary conditions and a horizontal resolution of 250 m. The depth of the domain is 2 km with 41 z-levels whose thicknesses increases from 10 m at surface to 100 m near the bottom. The model transports oxygen which is influenced by the air-sea gas transfer only. Uniform cooling of varying duration is applied at the surface in 4 sensitivity runs (Table 1). Bubble injection is included in 4 additional runs, and the results are shown in Fig. S2. Diffusive oxygen flux is applied at the surface, and the surface wind speed is fixed. By sampling a wide range of cooling rates from 400 to 4,000 W/m^2, these calculations explore the different

Table 1. Parameters used for the non-hydrostatic sensitivity experiments. The total heat loss is the same in all experiments. The 10 m wind speed is used only for the purpose of calculating the gas transfer coefficient (G) and the bubble-mediated gas flux. These runs are a subset of the simulations in Sun et al. (2017).

Run	period ($days$)	-Q ($W\ m^{-2}$)	$|u_{10}|$ ($m\ s^{-1}$)
$c06w15$	6	4000	15
$c15w15$	15	1600	15
$c30w15$	30	800	15
$c60w15$	60	400	15

responses of entrainment and air-sea equilibration. The effect of the biological pump is not directly simulated, and we focus only on conditions relevant to winter-time convection. The biological impact is implicitly included in the initial condition of the subsurface O_2 distribution, which modulates the effect of entrainment. As the model is initialized in fall (October), the initial vertical gradient of O_2 reflects the summer-time productivity and respiration in the interior ocean. Further details on the set-up can be found in Sun et al. (2017).

3.2 Regional simulations

To further test our theoretical prediction, we also design a set of regional numerical simulations with the MITgcm. The model domain covers the Labrador Sea (Fig. 4) with 7.5 km horizontal resolution and 40 vertical layers ranging from 6.25 m (surface) to 250 m (near bottom). The K-profile parameterization (KPP) (Large et al., 1994) is used for vertical mixing, and an ecosystem model with 6 species of phytoplankton and 2 species of zooplankton is included (Pham & Ito, 2019). At the surface the model is forced by atmospheric fields from the reanalysis product ERA-Interim (Dee et al., 2011) and uses bulk formula. The physical open boundary conditions are interpolated from the Simple Ocean Data Assimilation ocean/sea ice reanalysis (SODA) 3.4.2 (Carton et al., 2018), while the boundary conditions of phosphate, nitrate, silicate and oxygen are provided by the World Ocean Atlas (WOA18) (Garcia et al., 2018a, 2018b). The boundary conditions for the remaining biogeochemical tracers are derived from the annual cycle pro-
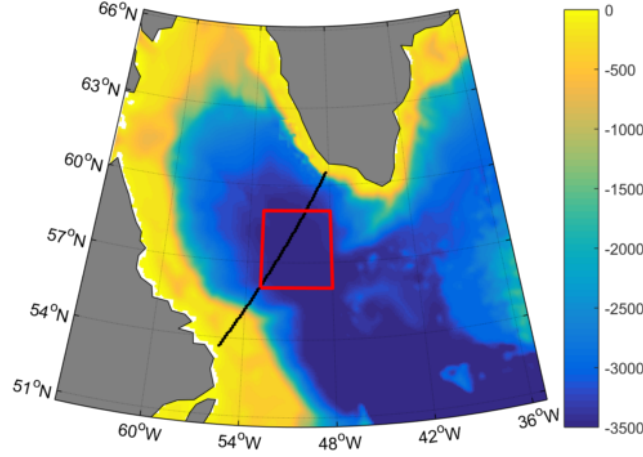
Figure 4. Topography of the simulated domain in the Labrador Sea. The black line indicates the WOCE Line AR7W. The red box shows the Central Labrador Sea (CLS) region defined as a box over (56 ^{o}N - 59 ^{o}N and 53 ^{o}W - 48 ^{o}W).

duced in the global simulation described in Pham and Ito (2019). The parameterization of surface oxygen flux is taken from Sun et al. (2017).

A set of 4 sensitivity runs is performed over the 8 year period from 2000 to 2007 . Fig. 5 compares the simulated potential density (σ_θ) and O_2 with those based on the cruise measurements along the World Ocean Circulation Experiment (WOCE) Line AR7W in May, 2000. This hydrography line cuts across the deep convective region of the Central Labrador Sea (CLS). Here we define the CLS region as the region over (56 ^{o}N - 59 ^{o}N and 53 ^{o}W - 48 ^{o}W) following Brandt et al. (2004) and Luo et al. (2011). The model shows reasonable skill at simulating the stratification and O_2 distribution in the Labrador Sea. There is a thin layer of cold and fresh water with low oxygen concentration, which is likely linked to sea ice. Our simulation does not include sea ice, so this water mass is not captured in the model. The model simulates a stronger than observed convective activity possibly due to its resolution (Tagklis, Bracco, et al., 2020), thus overestimates O_2 concentration.

The sensitivity experiments are performed modifying the surface boundary conditions. In the $CTRL$ and $lessC$ runs, only the diffusive oxygen flux is applied. The bubble injection flux is added in the $CTRLB$ and $lessCB$ experiments. In $lessC$ and $lessCB$ runs, the winter time (DJF) heat loss is reduced compared to the reanalysis data in the
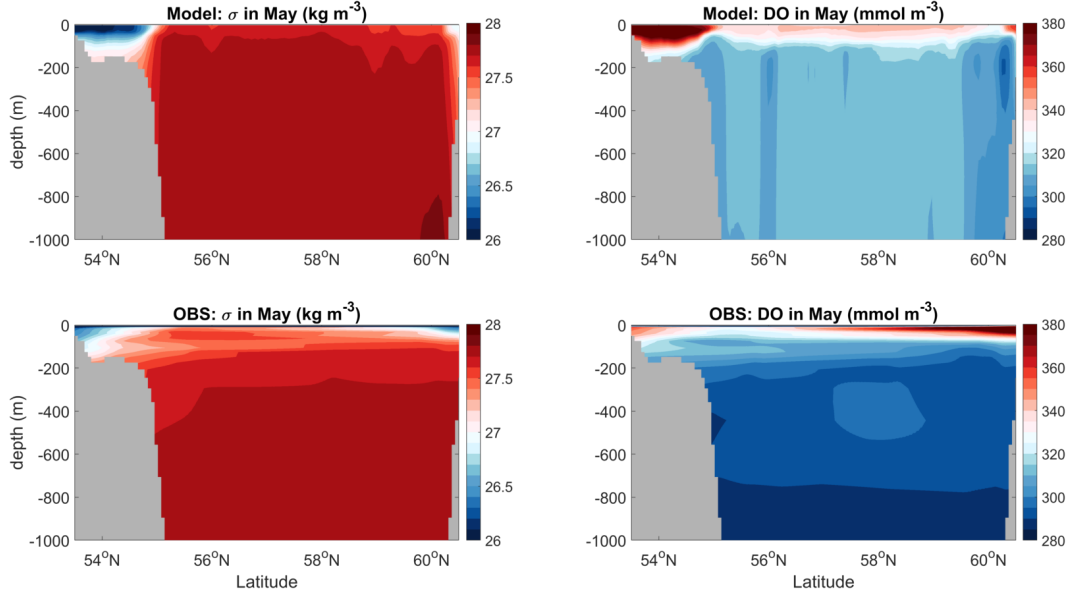
Figure 5. Comparison of the model simulated σ (A) and O_2 (B) and the observations from cruise measurements (CD) along the WOCE Line AR7W in May, 2000.

CLS region. This reduction is applied as a Gaussian function peaking at the center of the CLS. $CTRLB$ and $lessCB$ results are shown in Fig. S3

4 Results

4.1 The effect of atmospheric forcing

We now test the theoretical predictions of the O_2-OHC ratio using the non-hydrostatic simulations. In particular, the large η limit of Eq. 9 is relevant to the active deep convection of the non-hydrostatic runs. The physical set of this experiment is analogous to the the 1-D model (Fig. 6), and the theory predicts that the magnitude of the O_2-OHC ratio increases with time under constant cooling. In Fig. 6 each dot represents the results of a numerical simulation. As the cooling duration increases, the magnitude of cooling (Q) decreases so that the total heat loss remains the same for all cases. For a fixed amount of total heat loss, the seasonal O_2-OHC ratio is larger in magnitude when the cooling is applied over a longer period and follows a linear relationship (since $Q \propto t^{-1}$). The model output deviates from the linear relationship predicted by the large η limit because the surface oxygen flux can also affect the O_2 concentration. This misfit becomes more significant when the cooling is less intense and the cooling period is longer. In our
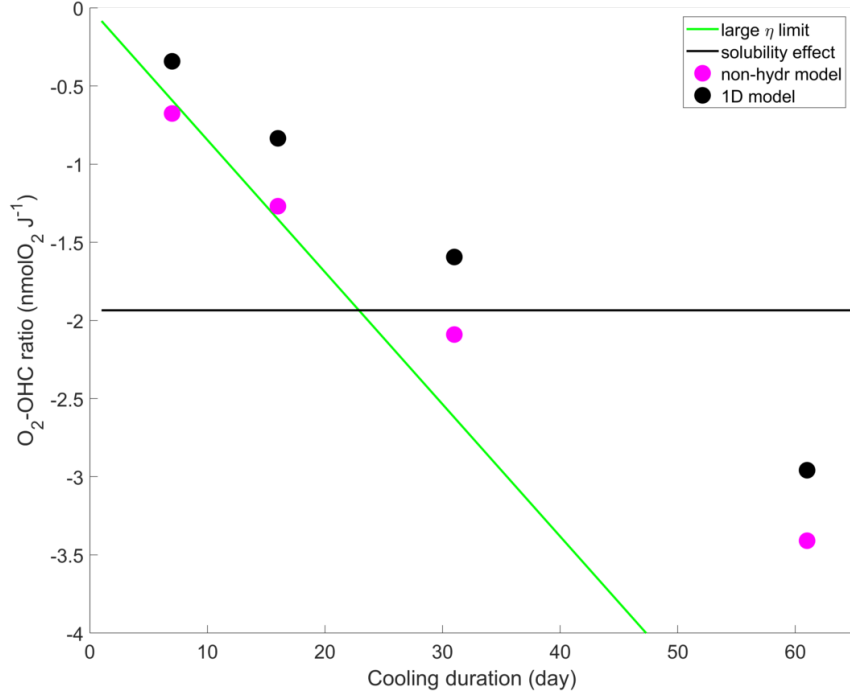
Figure 6. The seasonal O_2-OHC ratio as a function of cooling duration from the non-hydrstatic simulations compared with the solutions of the 1-D convective adjustment model.

model configuration, the surface flux can be extremely strong when the cooling period is short, which makes the O_2-OHC ratio even smaller than the solubility effect. Under these extreme conditions, the bottleneck is the finite gas exchange timescale of the air-sea oxygen flux. For a cooling time of $\sim$20 days or shorter, there is not enough time for the surface water O_2 concentration to respond to the increased air-sea flux. The solubility increase due to the cooling is faster than the increase of O_2 due to the air-sea gas exchange, and the O_2 content significantly lags behind the heat loss. While this situation may be applicable to an individual convective event, in reality the cool season generally lasts for several months, and the average cooling will not be as intense, so an extremely negative O_2-OHC ratio is unlikely.

As the cooling period gets longer, the absolute value of the O_2-OHC ratio increases. The theoretical magnitude of the seasonal O_2-OHC ratio is always greater than the numerical model outputs, as expected. The results from the vertical 1-D model and the non-hydrostatic model are similar, but the non-hydrostatic model shows a slightly larger magnitude of the O_2-OHC ratio with $\sim$-2.1 $nmolO_2/J$ for 30 days of cooling, which is close to the temperature-solubility relationship. For 60 days of cooling, magnitude increases

significantly reaching about -3.5 $nmolO_2/J$. In reality, the cool period can last longer than 60 days, so the amplitude of the O_2-OHC ratio can be greater than -3.5 $nmolO_2/J$ depending on the length and intensity of the heat loss. This demonstrates the complexity of the factors controlling the O_2-OHC ratio, as changes in atmospheric forcing alone can be conductive to very different outcomes.

4.2 Interannual variability of the O_2-OHC ratio

Given the role of the atmospheric forcing, the analysis of the multi-year, three-dimensional (3-D) simulations of the Labrador Sea is important because it is forced with realistic surface boundary conditions from meteorological reanalysis datasets. Unlike the vertical 1-D and non-hydrostatic model, this model uses realistic boundary conditions and simulates the full seasonal cycle as well as the biogeochemical sources and sinks of oxygen. Fig. 7 shows the seasonal mean surface oxygen flux (F) as a function of the mean cooling rate Q over the winter months (DJF) over seven convective seasons, from the 2000-2001 one to the 2006-2007. Each dot represents the winter oxygen and heat fluxes, seasonally (DJF) averaged for each of the 7 years. The blue circles are for the $CTRL$ run, and the red circles represent the $lessC$ run.

The values of k_T and $k_{\delta O2}$ are the regression coefficients of potential temperature and δO_2 in early December calculated as a function of depth in the $CTRL$ run. The model parameterizes G based on the daily atmospheric winds. In order to make a comparison with the theory /addunder small and large η limits, a representative constant G is estimated from the regression of winter time oxygen diffusive gas exchange and surface δO_2. Varying wind speed allows the gas exchange rate G to vary in the model simulations, and it may affect the interannul O_2-OHC ratio. To include the wind impact in the theoretical estimation, we must account for the relation between wind speed and the surface heat flux. As a first order approximation, we assume that the variation of the heat flux is mainly controlled by the change of sensible and latent heat, which are proportional to the surface wind speed. In our model simulation, G is proportional to the square of surface wind speed, and thus a quadratic function of the surface heat flux. After determining the coefficients from the regression between the mean gas exchange coefficient the mean heat flux in each winter in the regional simulations, we can have a large η limit estimation reflecting the varying G. The duration of the event is set to be 3 month as DJF is investigated here.
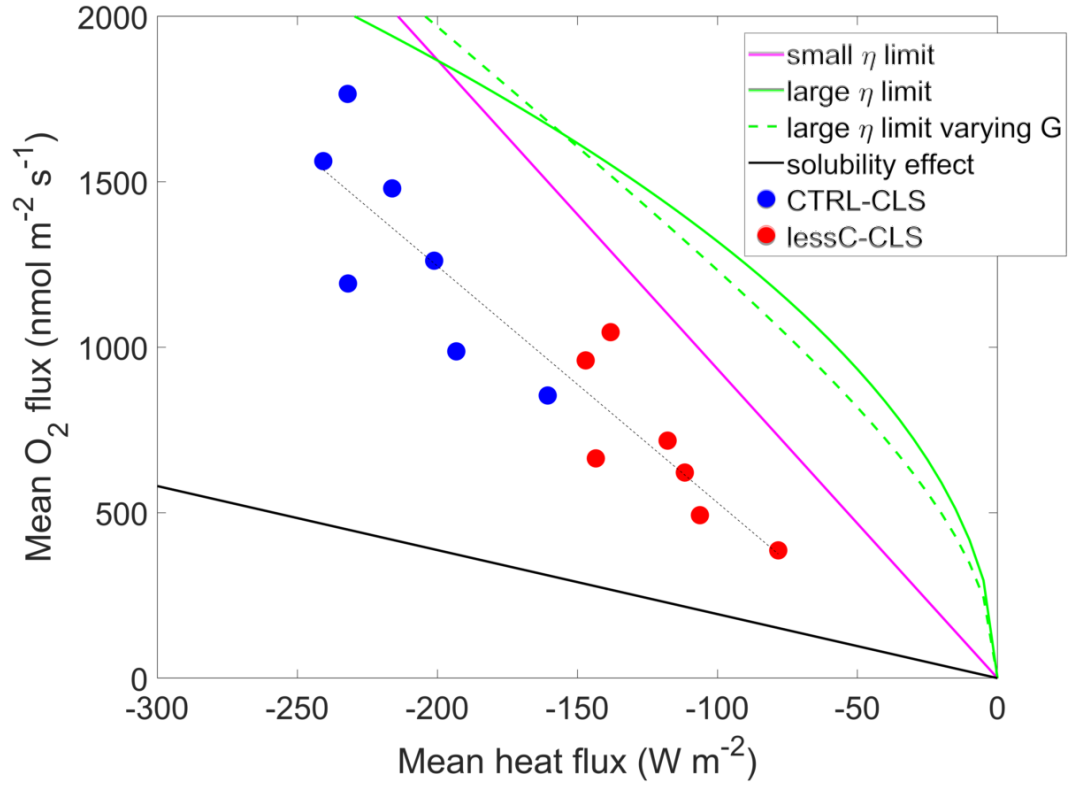
Figure 7. Mean air-sea oxygen flux as a function of mean surface heat flux over 7 different winters (from DJF between 2000 and 2001 to DJF between 2006 and 2007) in the CLS from the regional simulations compared with the theoretical predictions under different assumptions.The thin dashed black line is the linear fitting for all 14 points ($CTRL$ and $lessC$).

The outcome of the 3-D simulation is bounded by the theoretical predictions for the solubility effect (black) and the large η limit(green, and dashed green for the estimation with varying G). The oxygen fluxes mostly lie above the lower boundary defined by the solubility effect alone and below the large η limit. The small η limit suggests constant O_2-OHC ratio as shown in Eq.6. The large η limit predicts a non-linear relationship between the heat flux and oxygen flux (Eq.9). A varying G reduces the large η limit estimation of oxygen uptake when the cooling and wind are both weak, and increases the the estimation when the cooling and wind are strong. The stratification and vertical O_2 distribution vary among different years, so it is difficult to make exact comparison with the theory, but Fig. 7 shows a quasi-linear relationship between the mean rate of cooling and the oxygen uptake in the CLS region. It is also an open domain, and the lateral transport is clearly important for the regional oxygen budget and the evolution of O_2 concentrations in the mixed layer. Furthermore, in the regional set-up, the stratification is controlled not only by temperature but also by salinity and freshwater fluxes at the ocean surface. All these factors contribute to the O_2-OHC ratio interannual differences.

For predicting the future evolution of the O_2 inventory, the sensitivity of the total oxygen uptake to changes in heat fluxes is most important. Under the weak and large η limits, the interannual O_2-OHC ratio can be calculated following Eq. 6 and 10. Under the small η limit, the ratio is independent of the heat flux strength, while it is proportional to $(-Q)^{-1/2}$ under the large η limit, indicating a smaller ratio for strong cooling as shown in Fig. 7. Taking the variation of G into consideration overall increases the absolute value of the estimated interannual O_2-OHC ratio. Another factor to consider is the variability in the initial profiles of temperature and O_2 among cases and years. For the small η limit, larger vertical gradient of oxygen and weaker stratification will result in larger amplitude of O_2-OHC ratio. For the large η limit, larger k_T also implies larger ratio amplitude for a given $\frac{k_{\delta O2}}{k_T}$.

Plugging in the mean $k_{\delta O2}$ and k_T estimated from different simulations, the small η limit slightly overestimates the ratio, while the large η limit always predicts ratios that are too low (Table 2). By including the variation of G in the large η limit, the estimation becomes larger and closer to the model simulation. Relatively, the small η limit fits better the behavior of the regional model, which suggests that the small η limit is a potentially good estimation for the interannual O_2-OHC ratio. A possible explanation is

Table 2. Regression coefficient ($nmol O_2\,J^{-1}$) between the mean surface oxygen flux and heat flux over DJF in 7 different convective seasons (2001-2007) in the CLS compared with the theoretical prediction under small η (Eq. 6) limit, large η (Eq. 10) limit and large η limit with varying G (Eq. S21) using the mean vertical gradient of potential temperature and δO_2 extrapolated from different regional simulations.

Run	$\frac{d(Ft)}{d(Qt)}$	Eq. 6	Eq. 10	Eq. S21	k_T ($^oC\,m^{-1}$)	$k_{\delta O2}$ ($mmol\,m^{-4}$)
$CTRL$	-9.42	-9.49	-4.55	-7.25	5.27×10^{-4}	1.65×10^{-2}
$lessC$	-8.04	-8.88	-5.89	-7.32	5.77×10^{-4}	1.66×10^{-2}

that, even though a few intense convective events may happen during the winter, the relative strength of surface oxygen flux and entrainment may be closer to the small η limit when averaged for the whole 3-month period, at least in the years considered, all characterized by relatively weak convection in the Labrador Sea (Luo et al., 2014; Yashayaev & Loder, 2016). According to the small η limit, we would expect weaker interannual O_2-OHC ratio under a warmer climate ($lessC$) , which is also suggested by the model simulations, given that stratification (k_T) increases more than the oxygen gradient ($k_{\delta O2}$).

5 Discussion

In this work, we investigated the relationship between the surface oxygen flux and the heat flux during deep convection events. This relationship is fundamental to the O_2-OHC ratio in the ocean interior. Our results suggest that both the surface forcing and the vertical gradient of potential density and oxygen can alter the O_2-OHC ratio during convective events. The relative strength of stratification and the oxygen gradient may be the key factor to estimating the interannual O_2-OHC ratio.

The O_2-OHC ratio of calculated from our Labrador Sea simulation is larger than global estimates from ocean climate models (Keeling et al., 2010; Ito et al., 2017), but in broad agreement with the observational estimate of the O_2-OHC ratio for the North Atlantic Deep Water (NADW) in Keeling and Garcia (2002) (7.5 - 10 $nmol O_2\,J^{-1}$). When the model is run without bubble injection, the O_2-OHC ratio is -9.42 $nmol O_2\,J^{-1}$. Its magnitude increases to -11.20 $nmol O_2\,J^{-1}$ when the bubble (injection) flux is included.

470 Including the bubble-mediated flux increases the O_2-OHC ratio by $\sim$20%, in qualitative

471 agreement with Atamanchuk et al. (2020). As the bubble injection contribution can be

472 compensated by the decrease in diffusive gas exchange due to the elevated surface sat-

473 uration state when the vertical mixing is weak (Sun et al., 2017), its influence is more

474 significant under stronger cooling conditions (Fig. S1, S2 and S3). Additionally, the bubble-

475 mediated flux can alter the vertical gradient of O_2, so including bubble injection can im-

476 prove the simulation of the O_2-OHC ratio. Nevertheless, adding the bubble related oxy-

477 gen flux does not change our conclusions.

478 Despite its simplicity, the small η limit estimates the interannual O_2-OHC ratio re-

479 markably well in comparison to our regional numerical simulations. This suggests that

480 the climatological vertical gradients of potential density and O_2 are important in pre-

481 conditioning the interannual variability of the O_2-OHC ratio. Eq. 6 indicates a possi-

482 ble approach to estimate the local O_2-OHC ratio using the vertical gradients of temper-

483 ature and O_2, without direct measurement of the surface oxygen and heat flux when-

484 ever vertical mixing is mainly driven by thermal forcing. Based on the mean gradients

485 of temperature and O_2 from WOA18, the O_2-OHC ratio is estimated as -9.24 $nmolO_2\,J^{-1}$.

486 This value could be smaller if salinity gradient was included in the estimate of stratifi-

487 cation. On the other hand, the surface salinity forcing (e.g. brine rejection) will increase

488 the O_2-OHC ratio by causing more vertical mixing (thus more air-sea oxygen flux) with-

489 out changing the OHC. Further studies are needed to explore how the O_2-OHC ratio will

490 change in the future by taking the haline forcing on stratification into consideration. Our

491 regional simulations of the Labrador Sea show lower interannual O_2-OHC ratio when sur-

492 face cooling is reduced, consistent with the prediction from Plattner et al. (2002). Our

493 theory and model suggest that it is likely due to the stronger vertical gradient of poten-

494 tial temperature. These gradients are maintained by the ocean stratification, circulation

495 and the biological pump. In a warming climate, k_T is bound to increase due to the in-

496 creasing stratification, leading to a decrease in O_2-OHC ratio holding everything else con-

497 stant. However, over multiple decades, $k_{\delta O2}$ will also increase due to greater oxygen uti-

498 lization (Keeling et al., 2010; Ito et al., 2017), which can compensate the increase of k_T

499 and it may complicate our projection of the O_2-OHC ratio. Furthermore, a recent study

500 by Tagklis, Ito, and Bracco (2020) showed that the slowdown of the Atlantic Meridional

501 Overturning Circulation reduces the basin-scale upper ocean nutrient inventory, mod-

erating the oxygen loss. Such changes in the large-scale nutrient transport can alter the long-term change in the vertical gradient of O_2, and further affect the O_2-OHC ratio.

In a future warming climate, the overall change in the O_2-OHC ratio will be determined by the competition of changes in stratification and vertical oxygen gradient. Despite the simplicity of the theoretical model and the extreme assumption, the small η limit provides a reasonable first order prediction for the interannual O_2-OHC ratio. Changes of the stratification and O_2 gradient may be important indicators for the rate of deoxygenation in warming scenarios.

References

Atamanchuk, D., Koelling, J., Send, U., & Wallace, D. (2020). Rapid transfer of oxygen to the deep ocean mediated by bubbles. *Nature Geoscience*, 1–6.

Bopp, L., Le Quéré, C., Heimann, M., Manning, A. C., & Monfray, P. (2002). Climate-induced oceanic oxygen fluxes: Implications for the contemporary carbon budget. *Global Biogeochem. Cycles*, *16*. doi: 10.1029/2001GB001445

Brandt, P., Schott, F. A., Funk, A., & Martins, C. S. (2004). Seasonal to interannual variability of the eddy field in the labrador sea from satellite altimetry. *Journal of Geophysical Research: Oceans*, *109*(C2).

Carton, J. A., Chepurin, G. A., & Chen, L. (2018). Soda3: a new ocean climate reanalysis. *Journal of Climate*, *31*(17), 6967–6983.

Clarke, R. A., & Gascard, J. C. (1983). The formation of labrador sea-water .1. large-scale processes. *Journal of Physical Oceanography*, *13*(10),

1764-1778. Retrieved from `<GotoISI>://WOS:A1983RU25500002` doi: 10.1175/1520-0485(1983)013⟨1764:tfolsw⟩2.0.co;2

Codispoti, L. A. (1995). Is the ocean losing nitrate? *Nature*, *376*(6543), 724.

Dee, D. P., Uppala, S. M., Simmons, A. J., Berrisford, P., Poli, P., Kobayashi, S., . . . Vitart, F. (2011). The era-interim reanalysis: configuration and performance of the data assimilation system. *Quarterly Journal of the Royal Meteorological Society*, *137*(656), 553-597. Retrieved from `<GotoISI>://WOS: 000290450900001` doi: 10.1002/qj.828

Garcia, H. E., Weathers, K., Paver, C. R., Smolyar, I., Boyer, T. P., Locarnini, R. A., . . . Reagan, J. R. (2018a). World ocean atlas 2018, volume 3: Dissolved oxygen, apparent oxygen utilization, and oxygen saturation. *edited by: Mishonov, A., NOAA Atlas NESDIS*, *83*, 38.

Garcia, H. E., Weathers, K., Paver, C. R., Smolyar, I., Boyer, T. P., Locarnini, R. A., . . . Reagan, J. R. (2018b). World ocean atlas 2018, volume 4: Dissolved inorganic nutrients (phosphate, nitrate and nitrate+nitrite, silicate). *edited by: Mishonov, A., NOAA Atlas NESDIS*, *84*, 35.

Gascard, J. C., & Clarke, R. A. (1983). The formation of labrador sea-water. part ii. mesoscale and smaller-scale processes. *Journal of Physical Oceanography*, *13*(10), 1779-1797. Retrieved from `<GotoISI>://WOS:A1983RU25500003` doi: 10.1175/1520-0485(1983)013⟨1779:tfolsw⟩2.0.co;2

Hall, T. M., Haine, T. W. N., Holzer, M., Lebel, D. A., Terenzi, F., & Waugh, D. W. (2007). Ventilation rates estimated from tracers in the presence of mixing. *Journal of Physical Oceanography*, *37*(11), 2599-2611. Retrieved from `<GotoISI>://WOS:000251741600002` doi: 10.1175/2006jpo3471.1

Ito, T., Follows, M., & Boyle, E. (2004). Is aou a good measure of respiration in the oceans? *Geophysical research letters*, *31*(17).

Ito, T., Minobe, S., Long, M. C., & Deutsch, C. (2017). Upper ocean o2 trends: 1958–2015. *Geophysical Research Letters*, *44*(9), 4214–4223. Retrieved from `http://dx.doi.org/10.1002/2017GL073613` (2017GL073613) doi: 10.1002/ 2017GL073613

Jones, H., & Marshall, J. (1993). Convection with rotation in a neutral ocean: A study of open-ocean deep convection. *Journal of Physical Oceanography*, *23*(6), 1009–1039.

Keeling, R. F., & Garcia, H. E. (2002). The change in oceanic o-2 inventory associated with recent global warming. *Proceedings of the National Academy of Sciences of the United States of America*, *99*(12), 7848-7853. Retrieved from `<GotoISI>://WOS:000176217700011` doi: 10.1073/Pnas.122154899

Keeling, R. F., Körtzinger, A., & Gruber, N. (2010). Ocean deoxygenation in a warming world. *Annual Review of Marine Science*, *2*, 199-229. Retrieved from `<GotoISI>://WOS:000273985300008` doi: 10.1146/Annurev.Marine.010908 .163855

Körtzinger, A., Schimanski, J., Send, U., & Wallace, D. (2004). The ocean takes a deep breath. *Science*, *306*(5700), 1337-1337. Retrieved from `<GotoISI>:// WOS:000225301600041` doi: 10.1126/science.1102557

Large, W. G., Mcwilliams, J. C., & Doney, S. C. (1994). Oceanic vertical mixing - a review and a model with a nonlocal boundary-layer parameterization. *Reviews of Geophysics*, *32*(4), 363-403. Retrieved from `<GotoISI>://WOS: A1994PT55700002` doi: Doi10.1029/94rg01872

Lazier, J., Hendry, R., Clarke, A., Yashayaev, I., & Rhines, P. (2002). Convection and restratification in the labrador sea, 1990-2000. *Deep-Sea Research Part I-Oceanographic Research Papers*, *49*(10), 1819-1835. Retrieved from `<GotoISI>://WOS:000179693300007` doi: 10.1016/s0967-0637(02)00064-x

Luo, H., Bracco, A., & Di Lorenzo, E. (2011). The interannual variability of the surface eddy kinetic energy in the labrador sea. *Progress in Oceanography*, *91*(3), 295-311. Retrieved from `<GotoISI>://WOS:000295760900007` doi: 10.1016/ j.pocean.2011.01.006

Luo, H., Bracco, A., & Zhang, F. (2014). The seasonality of convective events in the labrador sea. *Journal of Climate*, *27*(17), 6456–6471.

Marshall, J., Adcroft, A., Hill, C., Perelman, L., & Heisey, C. (1997). A finite-volume, incompressible navier stokes model for studies of the ocean on parallel computers. *Journal of Geophysical Research: Oceans*, *102*(C3), 5753–5766.

Marshall, J., Hill, C., Perelman, L., & Adcroft, A. (1997). Hydrostatic, quasi-hydrostatic, and nonhydrostatic ocean modeling. *Journal of Geophysical Research: Oceans*, *102*(C3), 5733–5752.

Marshall, J., & Schott, F. (1999). Open-ocean convection: Observations, theory, and models. *Reviews of Geophysics*, *37*(1), 1-64. Retrieved from `<GotoISI>://`

WOS:000078534000001 doi: 10.1029/98rg02739

Matear, R. J., Hirst, A. C., & McNeil, B. I.   (2000).   Changes in dissolved oxygen in the Southern Ocean with climate change.   *Geochem. Geophys. Geosyst.*, *1*, 1050-12. doi: 10.1029/2000GC000086

Morel, F., & Price, N.   (2003).   The biogeochemical cycles of trace metals in the oceans. *Science*, *300*(5621), 944–947.

Pham, A. L., & Ito, T. (2019). Ligand binding strength explains the distribution of iron in the north atlantic ocean.   *Geophysical Research Letters*, *46*(13), 7500–7508.

Pickart, R. S., Torres, D. J., & Clarke, R. A.   (2002).   Hydrography of the labrador sea during active convection.   *Journal of Physical Oceanography*, *32*(2), 428-457.   Retrieved from `<GotoISI>://WOS:000173976500005`   doi: 10.1175/1520-0485(2002)032⟨0428:hotlsd⟩2.0.co;2

Plattner, G.-K., Joos, F., & Stocker, T. F.   (2002).   Revision of the global carbon budget due to changing air-sea oxygen fluxes.   *Global Biogeochem. Cycles*, *16*. doi: 10.1029/2001GB001746

Pörtner, H. O., & Knust, R.   (2007).   Climate change affects marine fishes through the oxygen limitation of thermal tolerance. *science*, *315*(5808), 95–97.

Schmidtko, S., Stramma, L., & Visbeck, M. (2017). Decline in global oceanic oxygen content during the past five decades. *Nature*, *542*(7641), 335–339.

Sun, D., Ito, T., & Bracco, A. (2017). Oceanic uptake of oxygen during deep convection events through diffusive and bubble-mediated gas exchange.   *Global Biogeochemical Cycles*, *31*(10), 1579–1591.

Tagklis, F., Bracco, A., Ito, T., & Castelao, R.   (2020).   Submesoscale modulation of deep water formation in the labrador sea. *Scientific reports*, *10*(1), 1–13.

Tagklis, F., Ito, T., & Bracco, A.   (2020).   Modulation of the north atlantic deoxygenation by the slowdown of the nutrient stream.   *Biogeosciences Discussions*, 1–22.

Talley, L. D., & McCartney, M. S.   (1982).   Distribution and circulation of labrador sea water.   *Journal of Physical Oceanography*, *12*(11), 1189-1205.   Retrieved from `<GotoISI>://WOS:A1982PP77700003`   doi: 10.1175/1520-0485(1982)012⟨1189:dacols⟩2.0.co;2

Yashayaev, I. (2007). Hydrographic changes in the labrador sea, 1960-2005. *Progress*

632   *in Oceanography*, *73*(3), 242-276. doi: 10.1016/j.pocean.2007.04.015

633   Yashayaev, I., Bersch, M., & van Aken, H. M.   (2007).   Spreading of the labrador

634   sea water to the irminger and iceland basins.   *Geophysical Research Let-*

635   *ters*, *34*(10).   Retrieved from `<GotoISI>://WOS:000246838200003`   doi:

636   10.1029/2006gl028999

637   Yashayaev, I., & Loder, J. W.   (2016).   Recurrent replenishment of labrador

638   sea water and associated decadal-scale variability.   *Journal of Geophys-*

639   *ical Research: Oceans*, *121*(11), 8095-8114.   Retrieved from `https://`

640   `agupubs.onlinelibrary.wiley.com/doi/abs/10.1002/2016JC012046`   doi:

641   10.1002/2016JC012046